

MRI-GUIDED HDR PROSTATE BRACHYTHERAPY IN STANDARD 1.5T SCANNER

CYNTHIA MÉNARD, M.D.,* ROBERT C. SUSIL, PH.D.,† PETER CHOYKE, M.D.,‡
GARY S. GUSTAFSON, M.D.,§ WILLIAM KAMMERER, M.D.,|| HOLLY NING, PH.D.,*
ROBERT W. MILLER, PH.D.,* KAREN L. ULLMAN, R.T.T.,* NANCY SEARS CROUSE, R.N.,*
SHARON SMITH, R.N.,* ETIENNE LESSARD, PH.D.,¶ JEAN POULIOT, PH.D.,¶ VICTOR WRIGHT, R.T.,#
ELLIOT McVEIGH, PH.D.,# C. NORMAN COLEMAN, M.D.,* AND KEVIN CAMPHAUSEN, M.D.*

*Radiation Oncology Branch, National Cancer Institute, Departments of †Radiology and ‡Anesthesia, Clinical Center, and ††Laboratory of Cardiac Energetics, National Heart, Lung, and Blood Institute, National Institutes of Health, Department of Health and Human Services, Bethesda, MD; ††Department of Biomedical Engineering, Johns Hopkins University School of Medicine, Baltimore, MD; §Department of Radiation Oncology, William Beaumont Hospital, Royal Oak, MI; ¶Department of Radiation Oncology, University of California, San Francisco, School of Medicine, San Francisco, CA

Purpose: Magnetic resonance imaging (MRI) provides superior visualization of the prostate and surrounding anatomy, making it the modality of choice for imaging the prostate gland. This pilot study was performed to determine the feasibility and dosimetric quality achieved when placing high-dose-rate prostate brachytherapy catheters under MRI guidance in a standard “closed-bore” 1.5T scanner.

Methods and Materials: Patients with intermediate-risk and high-risk localized prostate cancer received MRI-guided high-dose-rate brachytherapy boosts before and after a course of external beam radiotherapy. Using a custom visualization and targeting program, the brachytherapy catheters were placed and adjusted under MRI guidance until satisfactory implant geometry was achieved. Inverse treatment planning was performed using high-resolution T₂-weighted MRI.

Results: Ten brachytherapy procedures were performed on 5 patients. The median percentage of volume receiving 100% of prescribed minimal peripheral dose (V₁₀₀) achieved was 94% (mean, 92%; 95% confidence interval, 89–95%). The urethral V₁₂₅ ranged from 0% to 18% (median, 5%), and the rectal V₇₅ ranged from 0% to 3.1% (median, 0.3%). In all cases, lesions highly suspicious for malignancy could be visualized on the procedural MRI, and extracapsular disease was identified in 2 patients.

Conclusion: High-dose-rate prostate brachytherapy in a standard 1.5T MRI scanner is feasible and achieves favorable dosimetry within a reasonable period with high-quality image guidance. Although the procedure was well tolerated in the acute setting, additional follow-up is required to determine the long-term safety and efficacy of this approach. © 2004 Elsevier Inc.

Prostate cancer, Brachytherapy, MRI, Image guidance.

INTRODUCTION

Prostate cancer is the most common noncutaneous malignancy in men, with radiotherapy (RT) constituting the mainstay of definitive local therapy for patients with intermediate- and high-risk disease (1). Compared to low-risk subgroups, these patients are at greater risk of microscopic

extracapsular, seminal vesicle, or regional lymph node involvement and have a larger burden of disease in the prostate gland (2, 3). Evidence is mounting that local control rates can be improved by delivering higher boost doses of RT to the prostate gland in these patients (4–6).

Brachytherapy, designed and delivered with accurate anatomic reference, is well suited for dose escalation. By

Reprint requests to: Cynthia Ménard, M.D., Radiation Oncology Branch, National Cancer Institute, National Institutes of Health, Department of Health and Human Services, Bldg. 10, Rm. B3B69, 9000 Rockville Pike, Bethesda, MD 20892. Tel: (301) 496-9195; Fax: (301) 480-5439; E-mail: menardc@mail.nih.gov

Supported in part by U.S. Army Grant PC 10029, an NSF Engineering Research Center PER Grant, and in collaboration with Nucletron Inc.; Robert Susil is supported by an NIH MSTP fellowship; Cynthia Ménard is supported in part by an ASTRO fellowship.

Acknowledgments—The authors thank Nucletron, Inc. for instrumental research collaborations, USA Instruments for providing the endorectal imaging coils, Siemens Medical for providing portions of the coil immobilization arm, Dr. Robert J. Lederman for additional laboratory and scanner resources, Frank Harrington for developing the template and immobilization hardware, Dr. Huchen Xie for assistance in image processing, and the Urologic Oncology Branch at the NCI for their input and support.

Received Oct 15, 2003, and in revised form Jan 13, 2004.
Accepted for publication Jan 16, 2004.

virtue of the “inverse square” law, brachytherapy results in a much steeper dose gradient, and hence can achieve an improved therapeutic ratio compared with external beam RT (EBRT). The technique, however, demands a high level of accuracy and precision. Compared with ultrasonography, MRI provides far better visualization of the prostate and surrounding anatomy, making it the modality of choice for imaging the prostate gland (7). Given that accuracy in brachytherapy is largely dependent on the quality of the images, the rationale for using MRI during brachytherapy catheter placement and treatment planning is strong. MRI offers a three-dimensional (3D) data set, arbitrary imaging planes, and unparalleled soft tissue contrast.

Furthermore, MRI technology offers the unique possibility of integrating a wide range of biologic images to precise dosimetric maps within the gland and of studying the underlying molecular properties of images and the changes that occur during RT (8). Examples include, but are not limited to, dynamic contrast-enhanced MRI and MR spectroscopy. In this regard, high-dose-rate (HDR) temporary implants may offer an advantage over permanent seed implants, such that complex dose distributions can be achieved by optimizing the dwell times after catheter placement. Specific areas with a high burden of disease or with biologic features indicative of radioresistance within the prostate gland may be specifically targeted for higher dose delivery (9, 10).

For these reasons, we chose to address the challenges involved with performing HDR prostate brachytherapy in a standard 1.5T MRI scanner. Standard MRI scanners, as opposed to “open” scanner architectures, are cylindrical in shape and can pose significant challenges to patient interventions within the spatial constraints of the scanner bore. However, they afford greater image quality because of their higher magnetic and gradient field strengths. This is increasingly the case with the 3T magnets now becoming available for clinical use. Moreover, they are more widely available and can be used for diagnostic studies and are, therefore, more cost effective than specialty magnets.

We report our results from the pilot “run-in” phase of a two-stage clinical trial designed to determine whether HDR prostate brachytherapy implants performed in a standard 1.5T MRI scanner would result in favorable dosimetric profiles. In this pilot phase of the trial, we sought to develop and perfect our technique. Having demonstrated the feasibility and consistency in our implant dosimetry and technique, the trial will now proceed to an evaluation phase with a larger cohort of patients.

METHODS AND MATERIALS

Eligibility evaluation and preplanning

Patients with intermediate- and high-risk localized prostate cancer were eligible to enroll if their disease profile included either Gleason score >6 , or clinical stage greater than T2a (American Joint Committee on Cancer, 2002 edition), or prostate-specific antigen (PSA) level of ≥ 10 ng/

mL, with no evidence of distant metastatic disease. Staging investigations included PSA measurement, digital rectal examination, histopathologic review, diagnostic endorectal coil MRI of the prostate, and bone scan in those with high-risk disease. Patients unsuitable for general anesthesia or MRI were excluded, as were patients who had undergone transurethral resection of the prostate (TURP) in the preceding 6 months, who had a large TURP defect, or had significant urinary symptoms as reflected by a high (>18) International Prostate Symptom Score.

All eligible patients underwent preliminary MRI in the treatment position before enrollment to confirm adequate perineal access and the absence of pubic arch interference. Preliminary MRI evaluations and procedures were performed on a Siemens Sonata 1.5T MRI scanner with a 60-cm-diameter bore (Siemens Medical Systems, Erlangen, Germany). A custom-built MRI table overlay was designed to permit patient and device immobilization. The patient was positioned head first in the left lateral decubitus position (Fig. 1). An axillary roll was placed to prevent brachial plexopathy during prolonged immobilization. The patient's position was adjusted such that the shoulders and hips did not collide with the anterior edge of the bore, and perineal exposure was optimized. Immobilization was achieved with support cushions (Action Products, Hagerstown, MD), surgical tape, and Velcro straps securing the patient to the table overlay at the head, shoulder, chest, abdomen, legs, and feet.

After a digital rectal examination, an endorectal imaging coil (USA Instruments, Aurora, OH) modified with immobilization hardware and rigidly affixed perpendicular to a custom-designed perineal template was inserted and placed against the anterior rectal wall adjacent to the prostate gland. A custom-modified immobilization arm (Siemens Medical Systems, Erlangen, Germany) affixed the coil/template device to the table overlay. The patient was then advanced into the scanner bore until the prostate gland was positioned at the magnet isocenter. Three-plane scout images were acquired to verify the position and orientation of the endorectal coil/template assembly. The endorectal coil was adjusted until it was parallel to, and centered on, the urethra (right to left).

Using the MRI scanner's graphic user interface, an imaging plane parallel to the template face was prescribed and a 3D-Steady State Free Precession (SSFP) image volume (TR 4.4 ms, TE 2.2 ms, Flip Angle (FA) 56° , pixel bandwidth (BW) 560 Hz, field of view 25 cm, slice thickness 3 mm, 256×256 , 60 slices, Number of Averages (NEX) 1, scan time 1:20 min, and images corrected for gradient nonlinearity) covering the template, pubic arch, and prostate gland was acquired.

An image of a grid with 5-mm spacing representing the template was fused to the prostate MR images with custom software. These images were transferred to a treatment planning workstation (PLATO, Nucletron, Columbia, MD), where the pubic arch, prostate gland, urethra, and rectum

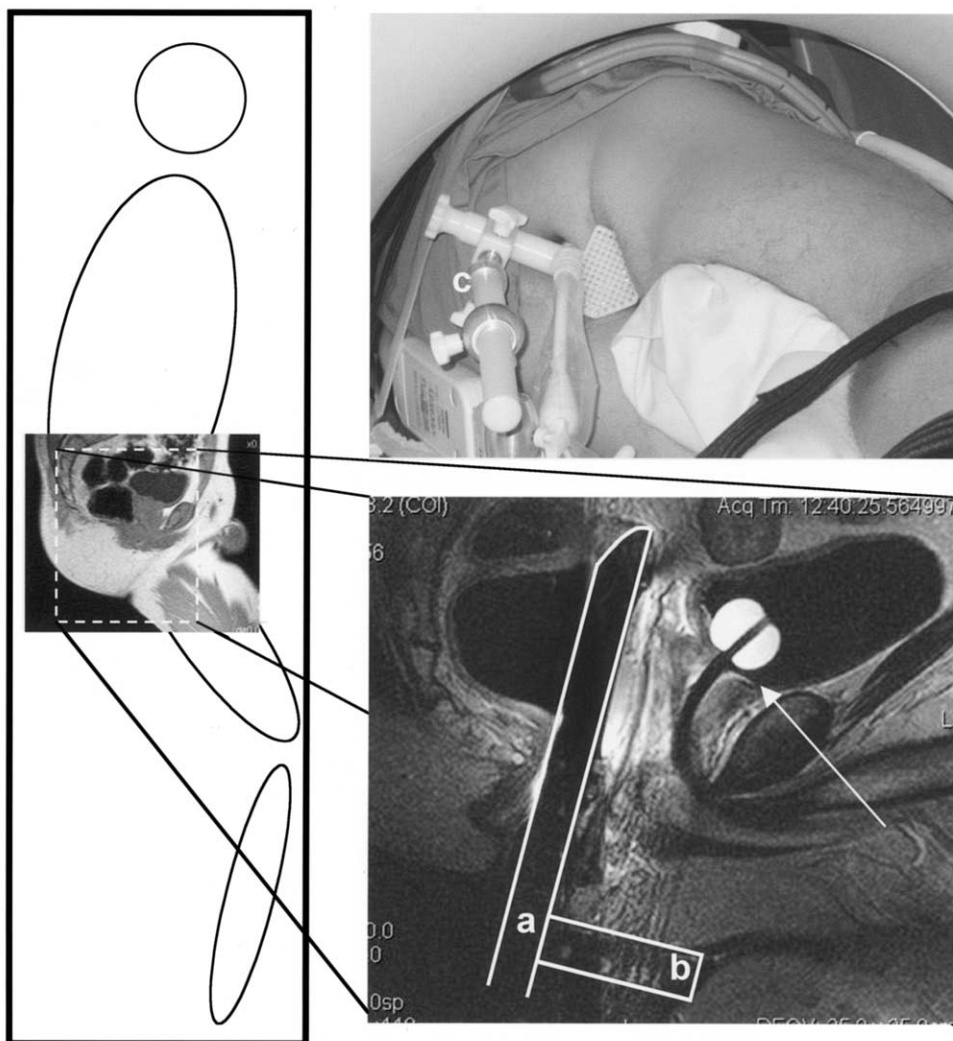


Fig. 1. Patient immobilized in left lateral position to maximize perineal exposure. Endorectal coil (a) perpendicular to template (b). Custom system placed against perineum, adjusted parallel to urethra under image guidance, and affixed to table with immobilization arm (c). Location of base of prostate clearly visualized (arrow).

were segmented. A peripheral catheter arrangement, respecting the template projection and pubic arch, was generated and arbitrarily optimized for target coverage. Those patients with pubic arch interference compromising target coverage were deemed ineligible and were excluded from the trial.

MRI-guided brachytherapy catheter placement

The patient underwent a bowel preparatory regimen and antibiotic prophylaxis (levofloxacin, 500 mg daily) 2 days before brachytherapy. The patient was placed under general endotracheal anesthesia for the entire procedure. A Foley catheter was inserted into the bladder and the balloon inflated with 10 mL of 0.5 mM gadolinium-diethylenetriamine pentaacetic acid. Once the bladder was completely drained, the Foley catheter was clamped to permit urine to collect in the bladder, thereby improving bladder mucosal definition on MRI. When satisfactory vital sign monitoring

was achieved in the MRI scanner, the patient was placed in the left lateral decubitus position and immobilized as described. Great care was taken to prevent positional injuries and to protect pressure points. Pneumatic compression stockings were applied to both lower extremities.

After digital rectal examination, the perineum was prepared and sterilely draped. The sterile endorectal imaging coil and template device was placed and affixed to the table overlay, and three-plane scout images were acquired, as described. After satisfactory device positioning, a parallel MRI plane was determined, and a 3D-SSFP image volume comprising the template, pubic arch, and prostate gland was acquired. These images were immediately sent to an adjacent personal computer workstation with a custom written image visualization and targeting program. The template position and orientation within the image volume was registered, and an intensity correction for the endorectal coil was applied on-line, as previously described (11). Those



Fig. 2. Magnetic resonance imaging (MRI) scanner room setup. Entire needle placement procedure performed inside of scanner room. Two physicians performed needle placement and one engineer controlled MRI scanner (via in-room console) and targeting and visualization application (via wireless keyboard and mouse). To ease visualization and planning, images were projected onto screen within scanner room.

needle paths potentially encroaching on the pubic arch and urethra were identified and marked, and a peripheral catheter arrangement was designed with the assistance of the preplan. Fast-spin-echo axial images of the prostate gland (TR 741 ms, TE 60 ms, ETL 7, pixel bandwidth 125 Hz/pixel, field of view 25 cm, slice thickness 4 mm, 256×256 , 12 slices, NEX 1, scan time 28 s, images corrected for gradient nonlinearity) were then acquired for improved target definition and to confirm the adequacy of the catheter arrangement. These images were projected with an LCD projector within the MR room to allow the operator more timely feedback of the catheter position (Fig. 2).

Catheters were placed by withdrawing the scanner table, inserting a coaxial MR-compatible needle (MRI Devices, WI; the depth that places the needle tip at the prostate base is displayed by the targeting program), advancing the table to the isocenter, and acquiring fast-spin-echo images to verify needle position accuracy. The transverse position of beveled coaxial needles can be adjusted within 5 mm of the projected target location by retracting the needle, rotating the bevel in the desired direction, and reinserting the needle. When a satisfactory needle position was confirmed with its tip at the base, a brachytherapy catheter (ProGuide, 5F, 294 mm, Nucletron) was inserted through the coaxial needle, which was then removed. Initially, one or two coaxial needles were inserted between each image verification sequence. As we gained confidence in the needle targeting accuracy of our system, up to five coaxial needles were typically inserted between each image verification sequence. When all brachytherapy catheters were satisfactorily placed, they were locked into position with template screws. For the first two procedures, cystoscopy was performed to verify that no catheter was perforating the urethral or bladder mucosa. In subsequent cases, this step was omitted because the location of the catheters in relation to the urethra and bladder base could be accurately identified by MRI alone.

The obturators within the brachytherapy catheters were removed, and most of the urine was drained from the bladder to prevent bladder distension, which could lead to

prostate displacement and bladder atony. The Foley catheter was then clamped again to create a distance between the dome of the bladder and the first dwell position, thereby reducing the radiation dose to the bladder mucosa. Final images were then acquired for treatment planning. These consisted of axial, sagittal, and coronal T_2 -weighted fast-spin-echo images (TE 121 ms, TR 3500 ms, ETL 9, pixel bandwidth 130 Hz/pixel, field of view 20 cm, slice thickness 3 mm, 256×256 , 26 slices, NEX 2, scan time 3.38 min, images corrected for gradient nonlinearity). All images were corrected for nonuniform imaging coil sensitivity and sent via network to an image server. The axial images were then loaded into the PLATO treatment planning workstation, and the other images were visualized (eFilm, Merge eFilm, WI) on an adjacent personal computer workstation.

After the acquisition of the treatment planning images, the obturators were replaced inside the brachytherapy catheters, and the patient was transferred by sliding the table overlay onto an MR-compatible stretcher while maintaining the left lateral decubitus position and without releasing any of the immobilization straps. Great care was taken to prevent pelvic movement with the transfer, and immobilization was maintained. The patient was brought to the shielded treatment room for RT. The Foley balloon MRI contrast was replaced with 10 mL of X-ray contrast (Isovue-300). A patient lateral portable X-ray was obtained to verify the needle tip location in relation to the Foley catheter balloon immediately before treatment. This X-ray was subjectively compared with a two-dimensional representation of the catheters and Foley balloon, generated from the treatment planning MRI in PLATO, in a plane approximating that of the portable X-ray (Fig. 3).

3D-MRI-based treatment planning, RT delivery, and recovery

A clinical target volume (CTV) comprising the prostate gland and any extracapsular disease visualized on the MRI was contoured, along with the urethra, rectal mucosa, bladder, and Foley catheter balloon. The location of the apex of the gland was verified on the sagittal and coronal images.

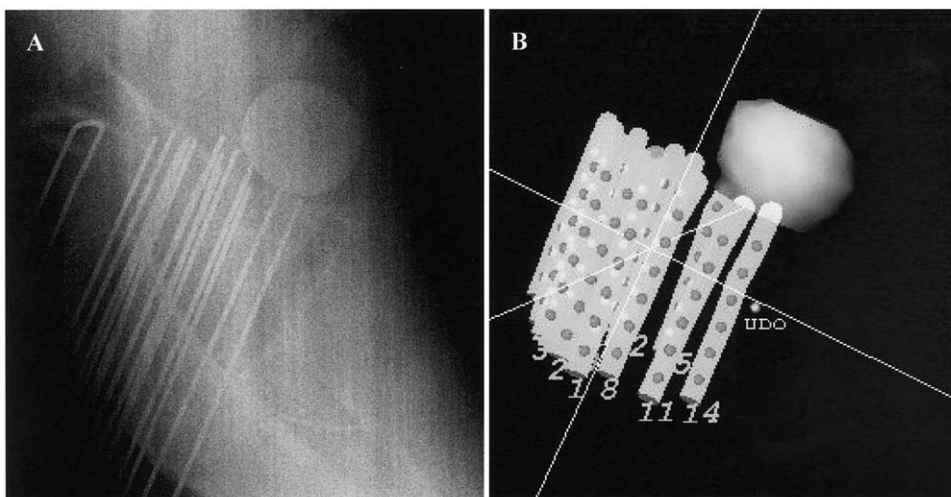


Fig. 3. (a) Diagnostic portable X-ray showing relationship between Foley balloon and brachytherapy catheters acquired immediately before radiotherapy delivery and compared with (b) surface-rendered image generated from treatment planning MRI. No appreciable motion of catheters was noted.

The 3D reconstructions of the brachytherapy catheters were manually performed on the axial MRI. Dwell time optimization was performed to achieve the following dosimetric parameters: target percentage of volume receiving 100% of prescribed minimal peripheral dose (V_{100}) $>90\%$, urethral $V_{150} <2\%$ and $V_{125} <20\%$, and rectal $V_{75} <2\%$. The guidelines were chosen to follow those previously published in the literature recommending a rectal dose of $<75\%$ and urethral dose of $<125\%$ of the prescription dose (12, 13). Because these studies defined the urethral dose at a point in the center of the urethra, our urethral constraints were modified to allow for a relatively larger urethral organ volume definition. At the inception of the trial, dwell time optimization was performed with “forward planning,” consisting of geometric computer optimization followed by manual isodose manipulations until a satisfactory plan was achieved. From the third procedure onward, “inverse planning” was performed with inverse planning-simulated annealing (IPSA) (14) (Nucletron, courtesy of Dr. J. Pouliot) in which dose constraints were applied to the target, urethra, bladder, and rectum and adjusted until a satisfactory plan was achieved.

If the above-defined dosimetric parameters were achieved, a dose of 1050 cGy was prescribed to the 100% isodose. If they were not achieved, but a urethral $V_{150} <2\%$, and rectal $V_{75} <5\%$ were obtained, 950 cGy was prescribed to the 100% isodose line (13). RT was delivered immediately after completion of treatment planning, and the catheters were then removed and pressure was applied to the perineum until hemostasis was achieved. All immobilization devices were removed, and the patient was placed in the supine position for recovery from general anesthesia. The Foley catheter was removed 1–2 h after RT delivery, and the patient was monitored for vital signs and urine output. The patient was discharged

when stable and able to void without difficulty. Antibiotic prophylaxis was continued for 7 days.

EBRT and follow-up

Computed tomography simulation was performed 1 day after the first brachytherapy procedure with the patient in the supine position. The patient was instructed to void before simulation. CT images of the pelvis were obtained, and treatment planning for EBRT was performed. For those patients with high-risk localized disease (Gleason score ≥ 8 , PSA ≥ 20 ng/mL, or Stage T3a or greater disease), the CTV included the prostate gland, seminal vesicles, and regional pelvic lymph nodes at risk. For all other patients with intermediate-risk localized disease, the CTV included the prostate gland and seminal vesicles. A planning target volume was obtained by adding a margin of 1.5 cm to the CTV. A dose of 4600 cGy was prescribed to the 100% isodose in 23 fractions, 200 cGy/d. Hormonal therapy was permitted during the trial at the discretion of the patient and treating physician and administered in a neoadjuvant, concurrent, and adjuvant fashion. During the last week of EBRT, or the week after EBRT, a second brachytherapy fraction was delivered in the same fashion.

At treatment completion, patients were instructed to return to clinic for follow-up evaluations at 1, 3, 6, 12, and 18 months, and yearly thereafter. The Radiation Therapy Oncology Group toxicity grades were documented at each follow-up visit.

RESULTS

To date, 10 MRI-guided prostate HDR brachytherapy procedures have been successfully performed on 5 patients. Nine patients have undergone the preplanning MRI eligibility evaluation, and all had satisfactory perineal exposure

Table 1. Patient characteristics

Age (y)	Height (cm)	Weight (kg)	Gland size (cm ³)	Gleason score	Pretreatment PSA (ng/mL)	Clinical stage*	ERC-MRI T stage	Lesion visualized on T ₂ W MRI	Risk group
63	188	89	38	7	6.0	T2a	T2c	Yes	Intermediate
50	177	90	29	9	11.2	T1c	T3a	Yes	High
52	189	101	29	7	5.8	T2a	T3a	Yes	Intermediate
60	174	68	35	7	8.3	T1c	T2c	Yes	Intermediate
68	167	75	47	7	7.4	T1c	T2c	Yes	Intermediate

Abbreviations: PSA = prostate-specific antigen; ERC = endorectal coil; T₂W = T₂-weighted.

* American Joint Committee on Cancer Staging System, 6th edition.

with no evidence of pubic arch interference. One patient was enrolled in the trial but was later removed when his first brachytherapy procedure was aborted owing to instability in the template fixation system, which was then modified. Of those screened, 2 patients opted not to enroll in the trial, and another patient was rendered ineligible because of a new diagnosis of bladder cancer. All 5 remaining patients were enrolled in the trial and completed their course of therapy. One patient was followed for 6 months, 3 patients for 3 months, and 1 patient for 1 month after therapy completion.

The patient and disease characteristics are described in Table 1. The prostate gland size as determined by treatment planning MRI obtained within 1 month of the first implant procedure ranged from 29 to 47 cm³. In 2 patients (with a gland size of 29 and 35 cm³), hormonal therapy was delivered during this interval, thereby potentially reducing the gland size. In all patients, lesions highly suspicious for malignancy could be visualized on MRI, and extracapsular disease was identified in 2 patients (Table 1). Figure 4 shows two representative examples of the MRI quality obtained to guide catheter placement and for treatment planning. The catheters appear as small black dots (signal void) without creating image artifacts. Areas of low intensity suspicious of malignancy and extracapsular extension were delineated in the procedural MRI, included in the target volume (purple), and encompassed by the 100% isodose line (yellow). The shape of the rectum conformed to the shape of the endorectal coil. All generated preplans met our dosimetric guidelines, with a median of 14 catheters.

The overall procedure time, determined from the time of anesthesia induction to extubation, has consistently improved as we have gained experience with this new procedure (Fig. 5). The introduction of IPSA for treatment planning and a larger number of coaxial needles placed for each image verification sequence were in part responsible for the improvement in the overall procedure time. However, most of the time gain can be attributed to the team's level of experience and efficiency at each additive step. The interventional MRI procedure time was approximately 90 min with the last procedure performed. No complications resulted from the anesthetic procedure, which was well tolerated. Given the low room temperatures dictated by the MRI system, great care was required to prevent hypothermia by

covering the patient with warm blankets. The mean needle targeting accuracy of our system was 2.1 mm, as previously described (11). On average, 15 catheters (range, 13–17 catheters) were placed during each procedure. Patient and/or template shift was detected once during seven procedures, so that the position and orientation of the template within the image volume was re-registered on-line before proceeding with the implant.

The urethra and prostate–bladder interface were clearly visualized on MRI (Fig. 1), which permitted precise placement of the catheter tips at the prostate and bladder base without puncturing the urethra or bladder mucosa. Cystoscopy was performed during the first two procedures and confirmed the MRI findings. With the exception of one procedure, no appreciable motion of the catheters occurred between the MRI scan acquired for treatment planning and the diagnostic X-ray obtained immediately before RT delivery despite patient transfers (Fig. 3). The pubic arch did not interfere in a prohibitive fashion, nor did clinically significant prostate gland motion occur to the left side of the pelvis in the lateral decubitus position.

The median V₁₀₀ achieved with this technique was 94% (mean, 92%; 95% confidence interval, 89–95%; Fig. 4). The urethral V₁₂₅ ranged from 0% to 18% (median, 5%), and the rectal V₇₅ ranged from 0% to 3.1% (median, 0.3%). The treatment planning and dwell time optimization was significantly shorter with IPSA compared with a “forward planning” approach, and the quality of the plan was consistently superior.

In all but one instance, patients were able to void without difficulty shortly after brachytherapy. In 1 patient, a prolonged procedure time with a distended bladder resulted in bladder atony, necessitating an indwelling Foley catheter for 2 days. Hematuria resolved spontaneously within 24–48 h in all cases. No infections or pressure injuries resulted from these procedures. One patient experienced transient Grade 1 sensory ulnar neuropathy 1 day after the brachytherapy procedure that was of uncertain significance. Five patients required oral analgesics after the procedure. For the duration of therapy, all 5 patients experienced Radiation Therapy Oncology Group Grade 2 acute urinary toxicity (requiring symptomatic support with tamsulosin), and Radiation Therapy Oncology Group Grade 1 acute GI toxicity

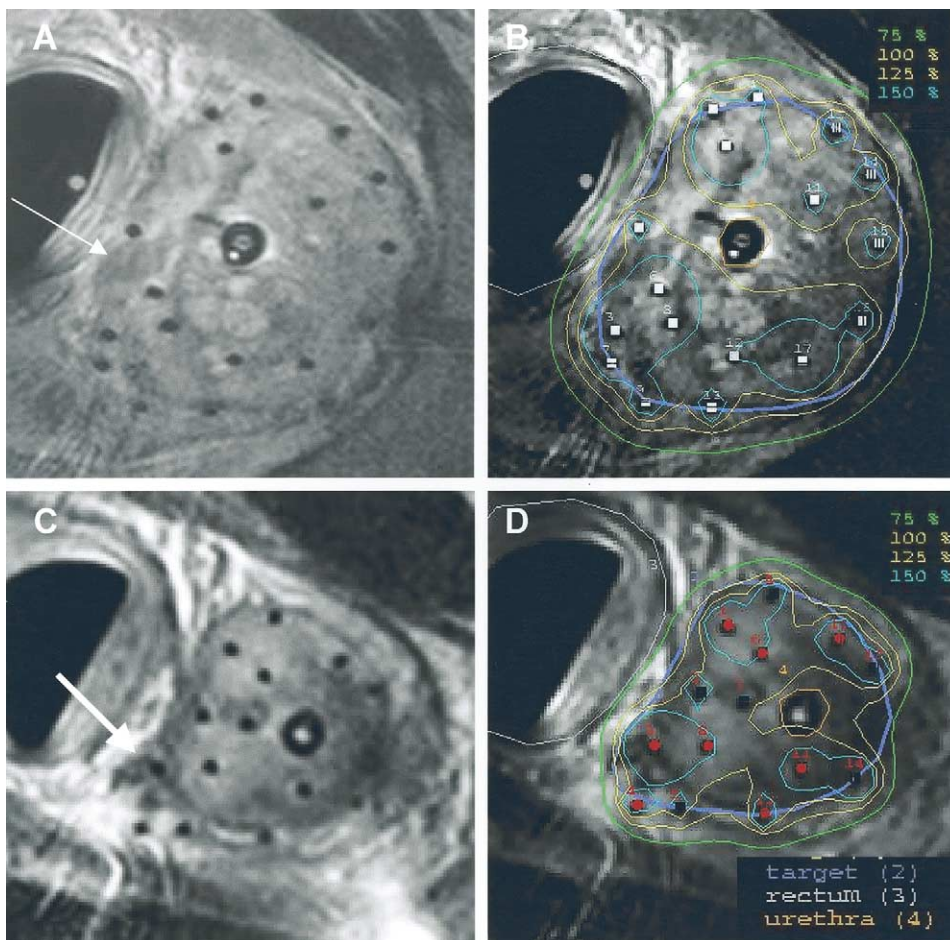


Fig. 4. Representative examples of MRI quality obtained to guide catheter placement and for treatment planning. Catheters appear as small black dots (signal void) without creating image artifacts. Areas of low intensity suspicious for malignancy (A, arrow) and extracapsular extension (C, arrow) can be delineated in procedural MRI included in target volume (purple) and encompassed by 100% isodose line (yellow).

consisting of increased bowel frequency. No Common Toxicity Criteria Grade 3 or worse acute toxicities occurred.

DISCUSSION

The high quality of anatomic images achieved with MRI technology (7) provides a strong rationale for the integration of MRI data with prostate brachytherapy, a technique that demands a high level of accuracy in target delineation. To this end, two general approaches are actively under investigation. The first involves performing brachytherapy procedures directly under the “real-time” guidance of MRI, which to date has focused on using MRI scanners with an “open” architecture. These systems have lent themselves well to interventional procedures because they afford a greater spatial freedom than conventional scanners. A technique for permanent seed implants of the prostate using an “open” MRI scanner has been designed, implemented, and reported (15–21). The results confirmed that transrectal ultrasound-guided implants may be improved on using MRI. However, because “open” MRI scanners have a significantly lower field strength and less gradient performance

than standard cylindrical magnets, less signal is available to generate the MRI data. This results in anatomic images of lesser quality than those acquired in standard MRI scanners and severe limitations to the integration of emerging techniques in biologic imaging (e.g., dynamic contrast-enhanced MRI, MR spectroscopy), all of which demand high signal levels.

A second approach is to “fuse” the diagnostic MRI data to the interventional images that guide needle placement, most commonly ultrasonography (22–24). This approach may be more broadly applicable, because ultrasound guidance for brachytherapy procedures demands less technical support and is readily available in most centers. However, it introduces registration errors and mandates two separate imaging sessions, one to acquire the diagnostic data and one for brachytherapy.

We chose to address the challenges involved with performing HDR prostate brachytherapy in a standard 1.5T MRI scanner for two main reasons. The first was to circumvent the errors introduced with deformable image registration of MRI data sets in an effort to improve the accuracy of anatomic target delineation, and in turn, the quality of the

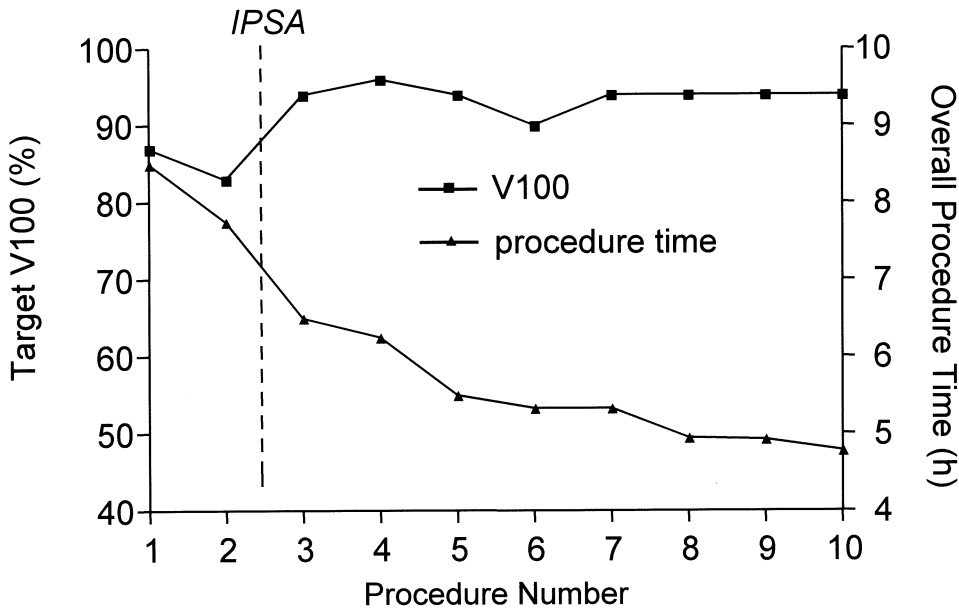


Fig. 5. Overall procedure time and target V_{100} through course of development of MRI-guided prostate brachytherapy in standard 1.5T scanner.

treatment. More importantly, however, we sought to establish a procedural platform in which new techniques for imaging tumor biology could be investigated simultaneously, compared with needle core tissue samples obtained under the same image coordinate reference, and directly applied to cancer therapy. Reducing the interval between the acquisition of the investigational imaging data, biopsy, and therapy, therefore, became important.

We have shown that HDR prostate brachytherapy in a 1.5T MRI scanner is feasible and can achieve favorable dosimetry in a reasonable period with exceptional image guidance. This procedure may offer a therapeutic advantage for those patients with extracapsular disease extension visualized on MRI, because extracapsular disease may be included in the radiation target volume. Our dosimetric results compared favorably with those published for a permanent seed implant technique performed under “open” MRI guidance, for which the median V_{100} was 96% (range, 89–99%) (21), and for HDR implants performed under ultrasound guidance with ISPA (mean V_{100} 96.3%) (25). However, this standard dosimetric measure of implant quality does not take into account the accuracy of the target delineation, which we surmise to be superior with the present technique. Also, the urethra and distal urethral muscles are more visible on MRI than on ultrasonography (images not shown); therefore, the urethral contours may be bigger on MRI. The same dosimetric index values (V_{125}) may result in less dose to the urethra using our technique.

Both the dosimetric parameters and the overall procedure time improved with the introduction of IPSA for treatment planning. As we continue to gain experience with this new technique, we anticipate additional improvements in the overall time required for this procedure. As we achieve

consistency in the overall procedure time, alternative anesthetic approaches such as spinal blocks and conscious sedation may be considered, because they may be better suited for some patients.

One of the challenges with this technique has been safe positioning and immobilization in the left lateral decubitus position. We chose this approach because it permitted maximal perineal exposure within the scanner bore size constraints. Although the scanner bore diameter is 60 cm, the space available in the AP dimension is limited to 45 cm because of the patient table. By placing patients in the lateral decubitus position, we took advantage of the much-needed additional 15 cm to better expose the perineum. For anesthetic considerations, this position was also favored over a prone position.

To our knowledge, no prior published experience is available to draw from regarding transperineal brachytherapy with patients in the left lateral decubitus position. A major concern with this position for a prolonged period is the stability of the position and the potential for brachial plexopathy and injuries to cutaneous pressure points. This risk, caused by traction on the brachial plexus from weight bearing on the dependent shoulder, can be reduced by placing an axillary roll that redistributes the weight to the chest wall (26). This standard technique is frequently applied during other surgical procedures performed in the lateral decubitus position. We have found that when sufficient time and care is taken during patient positioning and immobilization, pressure injuries and problems with patient shifts during the procedure can be largely circumvented.

Another concern was the position and stability of the prostate gland relative to the bony pelvis with patients in the left lateral position. To date, we have not experienced

difficulties with pubic arch interference and/or displacement of the prostate gland to the left side of the pelvis. Although limitations will surely exist in the eligible gland size and body habitus with this technique, we have not yet encountered them and they may not differ significantly from those applicable to a dorsal lithotomy approach. We suspect that the patient's shoulder width may become the most important limiting factor for this technique because of collision with the anterior edge of the scanner bore. Finally, our feasibility results to date must be confirmed with a larger cohort of patients.

As in all HDR brachytherapy procedures, preventing organ and/or catheter motion between the acquisition of the treatment planning images and RT delivery is of critical importance. Relatively small shifts in the catheter position relative to the target can potentially lead to important errors in delivery (27). In our case, the catheters were locked to the template, which was locked to the table overlay. The patient was kept under general anesthesia and in the same position until the treatment was delivered without releasing any of the immobilization devices. Patient transfer for RT delivery was achieved by simply sliding the table overlay from the MRI table to the stretcher. This table transfer, organ swelling, and a small amount of bladder filling in the 45–60-min interval between image acquisition and RT delivery could conceivably result in catheter shifts. For that reason, portable X-rays were obtained immediately before RT delivery, documenting the location of the catheter tips relative to the Foley catheter balloon. No subjective systematic shifts in catheter tip location relative to the Foley balloon between the MRI and X-ray images were appreciated. In the future, we hope to quantitate this observation by obtaining CT images in our department immediately before RT delivery.

Although this procedure is technically complex and requires more equipment and personnel resources than ultrasound-guided HDR prostate brachytherapy, it is ideally suited to the study of emerging MR-based biologic imaging techniques. Examples of novel imaging techniques currently under investigation include MR spectroscopic imaging (28, 29), dynamic contrast-enhanced MRI (30–33), diffusion-weighted imaging (34, 35), and bold oxygen level-dependent imaging (36), all of which require additional histopathologic and molecular validation before they are applied to the design of radiation targets. Once the diagnostic accuracy of these techniques is better determined, specific areas with a high burden of disease or with biologic features indicative of radioresistance within the prostate gland may be specifically targeted for higher radiation dose delivery. In essence, the basic knowledge gained from the clinical imaging research that can be conducted during this procedure may be translated directly back to patient care. This avenue of research is now being integrated with the HDR brachytherapy procedures and will be the subject of future work.

CONCLUSION

We have developed a technique for accurate transperineal prostate needle placements in a standard 1.5T MRI scanner that is an ideal platform for the validation and biologic study of various emerging molecular imaging techniques before and after RT, and allows for HDR brachytherapy with excellent target delineation (owing to high-quality MRI) and favorable radiation dosimetric profiles.

REFERENCES

1. American Cancer Society. Cancer facts & figures 2003. Atlanta, GA: American Cancer Society; 2003.
2. Lieberfarb ME, Schultz D, Whittington R, *et al*. Using PSA, biopsy Gleason score, clinical stage, and the percentage of positive biopsies to identify optimal candidates for prostate-only radiation therapy. *Int J Radiat Oncol Biol Phys* 2002;53:898–903.
3. Partin AW, Mangold LA, Lamm DM, *et al*. Contemporary update of prostate cancer staging nomograms (Partin tables) for the new millennium. *Urology* 2001;58:843–848.
4. Pollack A, Zagars GK, Smith LG, *et al*. Preliminary results of a randomized radiotherapy dose-escalation study comparing 70 Gy with 78 Gy for prostate cancer. *J Clin Oncol* 2000;18:3904–3911.
5. Zelefsky M, Fuks Z, Chan H, *et al*. Ten-year results of dose escalation with 3-dimensional conformal radiotherapy for patients with clinically localized prostate cancer. *Int J Radiat Oncol Biol Phys* 2003;57:S149–S150.
6. Nguyen KH, Horwitz EM, Hanlon AL, *et al*. Does short-term androgen deprivation substitute for radiation dose in the treatment of high-risk prostate cancer? *Int J Radiat Oncol Biol Phys* 2003;57:377–383.
7. Yu KK, Hricak H. Imaging prostate cancer. *Radiol Clin North Am* 2000;38:59–85.
8. D'Amico AV, Debruyne F, Huland H, *et al*. Innovative treatment for clinically localized adenocarcinoma of the prostate: the future role of molecular imaging. *Prostate* 1999;41:208–212.
9. Zaider M, Zelefsky MJ, Lee EK, *et al*. Treatment planning for prostate implants using magnetic-resonance spectroscopy imaging. *Int J Radiat Oncol Biol Phys* 2000;47:1085–1096.
10. Pickett B, Vigneault E, Kurhanewicz J, *et al*. Static field intensity modulation to treat a dominant intra-prostatic lesion to 90 Gy compared to seven field 3-dimensional radiotherapy. *Int J Radiat Oncol Biol Phys* 1999;44:921–929.
11. Susil RC, Camphausen K, Choyke P, *et al*. MRI-guided prostate interventions in a standard 1.5T magnet. *Magn Reson Med* 2004; In press.
12. Rodriguez RR, Demanes DJ, Altieri GA. High dose rate brachytherapy in the treatment of prostate cancer. *Hematol Oncol Clin North Am* 1999;13:503–523.
13. Martinez AA, Gustafson G, Gonzalez J, *et al*. Dose escalation using conformal high-dose-rate brachytherapy improves outcome in unfavorable prostate cancer. *Int J Radiat Oncol Biol Phys* 2002;53:316–327.
14. Lessard E, Pouliot J. Inverse planning anatomy-based dose optimization for HDR-brachytherapy of the prostate using fast simulated annealing algorithm and dedicated objective function. *Med Phys* 2001;28:773–779.
15. Cormack RA, D'Amico AV, Hata N, *et al*. Feasibility of

- transperineal prostate biopsy under interventional magnetic resonance guidance. *Urology* 2000;56:663–664.
16. D'Amico AV, Cormack R, Tempany CM, *et al.* Real-time magnetic resonance image-guided interstitial brachytherapy in the treatment of select patients with clinically localized prostate cancer. *Int J Radiat Oncol Biol Phys* 1998;42:507–515.
 17. D'Amico A, Cormack R, Kumar S, *et al.* Real-time magnetic resonance imaging-guided brachytherapy in the treatment of selected patients with clinically localized prostate cancer. *J Endourol* 2000;14:367–370.
 18. D'Amico AV, Tempany CM, Cormack R, *et al.* Transperineal magnetic resonance image guided prostate biopsy. *J Urol* 2000;164:385–387.
 19. D'Amico AV, Cormack RA, Tempany CM. MRI-guided diagnosis and treatment of prostate cancer. *N Engl J Med* 2001;344:776–777.
 20. Hata N, Jinzaki M, Kacher D, *et al.* MR imaging-guided prostate biopsy with surgical navigation software: Device validation and feasibility. *Radiology* 2001;220:263–268.
 21. Hurwitz MD, Cormack R, Tempany CM, *et al.* Three-dimensional real-time magnetic resonance-guided interstitial prostate brachytherapy optimizes radiation dose distribution resulting in a favorable acute side effect profile in patients with clinically localized prostate cancer. *Tech Urol* 2000;6:89–94.
 22. DiBiase SJ, Hosseinzadeh K, Gullapalli RP, *et al.* Magnetic resonance spectroscopic imaging-guided brachytherapy for localized prostate cancer. *Int J Radiat Oncol Biol Phys* 2002;52:429–438.
 23. Kaplan I, Oldenburg NE, Meskell P, *et al.* Real time MRI-ultrasound image guided stereotactic prostate biopsy. *Magn Reson Imaging* 2002;20:295–299.
 24. Zelefsky MJ, Cohen G, Zakian KL, *et al.* Intraoperative conformal optimization for transperineal prostate implantation using magnetic resonance spectroscopic imaging. *Cancer J* 2000;6:249–255.
 25. Lachance B, Beliveau-Nadeau D, Lessard E, *et al.* Early clinical experience with anatomy-based inverse planning dose optimization for high-dose-rate boost of the prostate. *Int J Radiat Oncol Biol Phys* 2002;54:86–100.
 26. Gonzalez Della Valle A, Salonia-Ruzo P, Peterson MG, *et al.* Inflatable pillows as axillary support devices during surgery performed in the lateral decubitus position under epidural anesthesia. *Anesth Analg* 2001;93:1338–1343.
 27. Hoskin PJ, Bownes PJ, Ostler P, *et al.* High dose rate after-loading brachytherapy for prostate cancer: Catheter and gland movement between fractions. *Radiother Oncol* 2003;68:285–288.
 28. Kurhanewicz J, Vigneron DB, Hricak H, *et al.* Three-dimensional H-1 MR spectroscopic imaging of the in situ human prostate with high (0.24–0.7-cm³) spatial resolution. *Radiology* 1996;198:795–805.
 29. Kurhanewicz J, Swanson MG, Nelson SJ, *et al.* Combined magnetic resonance imaging and spectroscopic imaging approach to molecular imaging of prostate cancer. *J Magn Reson Imaging* 2002;16:451–463.
 30. Knopp MV, Weiss E, Sinn HP, *et al.* Pathophysiologic basis of contrast enhancement in breast tumors. *J Magn Reson Imaging* 1999;10:260–266.
 31. Oyen RH. Dynamic contrast-enhanced MRI of the prostate: Is this the way to proceed for characterization of prostatic carcinoma? *Eur Radiol* 2003;13:921–924.
 32. Preziosi P, Orlacchio A, Di Giambattista G, *et al.* Enhancement patterns of prostate cancer in dynamic MRI. *Eur Radiol* 2003;13:925–930.
 33. Padhani AR, Gapinski CJ, Macvicar DA, *et al.* Dynamic contrast enhanced MRI of prostate cancer: Correlation with morphology and tumour stage, histological grade and PSA. *Clin Radiol* 2000;55:99–109.
 34. Issa B. In vivo measurement of the apparent diffusion coefficient in normal and malignant prostatic tissues using echo-planar imaging. *J Magn Reson Imaging* 2002;16:196–200.
 35. Gibbs P, Tozer DJ, Liney GP, *et al.* Comparison of quantitative T₂ mapping and diffusion-weighted imaging in the normal and pathologic prostate. *Magn Reson Med* 2001;46:1054–1058.
 36. Taylor NJ, Baddeley H, Goodchild KA, *et al.* BOLD MRI of human tumor oxygenation during carbogen breathing. *J Magn Reson Imaging* 2001;14:156–163.